CHINESE OPTICS LETTERS

Vol. 19, No. 3 | March 2021

Natural logarithm wavelength modulation spectroscopy

Shaomin Li (李绍民) and Liqun Sun (孙利群)*

State Key Laboratory of Precision Measurement Technology and Instruments, Department of Precision Instruments, Tsinghua University, Beijing 100084, China

*Corresponding author: sunlq@mail.tsinghua.edu.cn

Received December 4, 2020 | Accepted January 12, 2021 | Posted Online February 22, 2021

Natural logarithm wavelength modulation spectroscopy (ln-WMS) is demonstrated in this Letter. Unlike the conventional wavelength modulation spectroscopy (WMS)-2f technique, it is a linear method even for large absorbance, which is the core advantage of ln-WMS. The treating method used in ln-WMS is to take the natural logarithm of the transmitted intensity. In order to determine the proper demodulation phase, the η-seeking algorithm is introduced, which minimizes the absolute value of the first harmonic within the non-absorbing region. Subsequently, the second harmonic of the absorption signal is extracted by setting the demodulating phase as 2η. To illustrate the validity of ln-WMS, it was applied to water vapor experimentally. The result shows that even if the absorbance (base-e) is between 1.60 and 6.26, the linearity between ln-WMS-2f and volume fraction is still established. For comparison, measurement with conventional WMS-2f was also done, whose response no longer kept linearity. The η values retrieved in continuous measurements and the residuals were shown so as to evaluate the performance of the η-seeking algorithm. Time consumed by this algorithm was roughly 0.28 s per measurement. As an alternative WMS strategy, ln-WMS has a wide range of potential applications, especially where the absorbance is large or varies over a wide area.

Keywords: wavelength modulation spectroscopy; natural logarithm wavelength modulation spectroscopy; tunable diode laser absorption spectroscopy; large absorbance.

DOI: 10.3788/COL202119.031201

1. Introduction

Spectrometry-based techniques have frequently been used for gas detection[1,2] because of the advantages of high sensitivity, rapid response, etc.[3], of which wavelength modulation spectroscopy (WMS) is one of the most popular and widely used for environmental monitoring[4], breath analysis[5,6], combustion diagnostics[7–10], and so on. WMS is well known as means to increase the signal-to-noise ratio. The emitted wavelength of the diode laser is modulated at the frequency of several kilohertz or megahertz, and the absorption parameters of the absorber can be acquired by analyzing the harmonics demodulated from the absorption signal. The conventional WMS-2f technique has to linearly calibrate the second harmonic to standard gases of known concentrations for recovering the absolute gas concentration[11–13]. However, this technique is only applicable to low absorbance (lower than 0.05 typically[14]), because the WMS-2f theory is based on the linear approximation of the Beer–Lambert law, and, if the absorbance is not small enough, the approximation will not be established any more nor will the linearity. In recent years, some "calibration-free" methods have been proposed to measure gas parameters, including not only concentration but also temperature and pressure. For instance, Rieker *et al.*[14] proposed the calibration-free $nf/1f$ method to measure the gas temperature and concentration in harsh environments by minimizing the difference between the experimental value and the simulated one. McGettrick *et al.*[15] proposed the phasor decomposition method, which is a calibration-free WMS technique and utilizes the residual amplitude modulation (RAM) signal of the first harmonic for measuring concentration and pressure simultaneously. Contrasting with the conventional WMS-2f method, calibration-free WMS does not necessarily require the absorbance to be low, while it is capable of multi-parameter measurement.

In this Letter, a new branch of WMS technique— natural logarithm wavelength modulation spectroscopy (ln-WMS)—is proposed. It can be regarded as an improvement of the conventional WMS-2f technique. The implementation of ln-WMS is kind of similar to conventional WMS-2f — they both require prior calibration, and their hardware configurations are nothing different. What is different is that ln-WMS does not place theoretical limits of absorbance, which is because no low-order approximation is made to the Beer–Lambert law in the deduction of ln-WMS. Just as its name implies, the natural logarithm of the transmitted intensity is taken in ln-WMS, so the term that includes absorption information will not exist on the exponent

of e but will turn into a linear item instead; while in conventional WMS-2f theories, this is realized by substituting the Beer–Lambert law with its first-order approximation[12,13]. After confirming the demodulation phase with the η-seeking algorithm, the central value of the second harmonic (ln-WMS-2f) is linear to the path-integrated concentration of the absorber, with no limitation on absorbance.

2. Theories of ln-WMS

It being a branch of WMS, the diode laser is modulated in the same way as any WMS technique, i.e., the laser frequency and intensity are synchronously modulated by a sinusoidal signal. The frequency modulation (FM) and amplitude modulation (AM) can be expressed as[14,16–18]

$$\text{FM}: \nu(t) = \bar{\nu} + a\ \cos(\omega t + \psi + \phi), \tag{1}$$

$$\text{AM}: I_0(t) = \bar{I}_0[1 + i_1\ \cos(\omega t + \psi)], \tag{2}$$

where $\bar{\nu}$ refers to the laser central frequency, a is the FM depth, ω is the angular frequency of the modulation signal, $\bar{I}_0$ is the average intensity, i_1 is the linear AM amplitude (normalized by $\bar{I}_0$), ψ is the phase of AM, and ϕ is the phase difference between FM and AM. When a beam of a laser passes through absorbing samples, the transmitted intensity $I_t(t)$ is dominated by the Beer–Lambert law,

$$I_t(t) = I_0(t)\ \exp[-\alpha(\nu)CL], \tag{3}$$

where $\alpha(\nu)$ is the absorption coefficient at frequency ν; C and L represent the volume fraction of the absorber and the optical path length laser that passes through the absorber, respectively. The term $\ln(I_0/I_t)$ is called absorbance (base-e).

According to Eq. (3), the natural logarithm of $I_t(t)$ can be expressed as follows:

$$\begin{aligned}\ln\ I_t(t) &= \ln\ I_0(t) - \alpha(\nu)CL \\ &= \ln\ \bar{I}_0 + \ln[1 + i_1\ \cos(\omega t + \psi)] - \alpha(\nu)CL.\end{aligned} \tag{4}$$

In this way, the absorption term $\alpha(\nu)CL$ will become a linear term instead of an exponential term. According to the Taylor expansion of $\ln(1 + x)$ at $x = 0$,

$$\ln(1 + x) = \sum_{n=1}^{\infty} \frac{(-1)^{n+1}}{n} x^n, \qquad x \neq -1, \tag{5}$$

and the $\ln[1 + i_1\ \cos(\omega t + \psi)]$ term can be rewritten as

$$\begin{aligned}\ln[1 + i_1\ \cos(\omega t + \psi)] &= \sum_{n=1}^{\infty} \frac{(-1)^{n+1}}{n} i_1^n [\cos(\omega t + \psi)]^n \\ &= \sum_{n=0}^{\infty} p_n\ \cos[n(\omega t + \psi)].\end{aligned} \tag{6}$$

The terms p_n are polynomials of i_1, and we do not care for the specific value of p_n. The Fourier series of the time-dependent quantity $\alpha(\nu)CL$ can be expressed as

$$\alpha[\bar{\nu} + a\ \cos(\omega t + \psi + \phi)]CL = \sum_{k=0}^{\infty} H_k\ \cos[k(\omega t + \psi + \phi)], \tag{7}$$

where

$$H_0(\bar{\nu}, a) = \frac{CL}{2\pi} \int_{-\pi}^{\pi} \alpha(\bar{\nu} + a\ \cos\ \theta)\mathrm{d}\theta, \tag{8}$$

$$H_k(\bar{\nu}, a) = \frac{CL}{\pi} \int_{-\pi}^{\pi} \alpha(\bar{\nu} + a\ \cos\ \theta)\ \cos\ k\theta \mathrm{d}\theta, \qquad k \geq 1. \tag{9}$$

According to Eqs. (4), (6), and (7),

$$\begin{aligned}\ln\ I_t = \ln\ \bar{I}_0 &+ \sum_{n=0}^{\infty} p_n\ \cos[n(\omega t + \psi)] \\ &- \sum_{k=0}^{\infty} H_k\ \cos[k(\omega t + \psi + \phi)].\end{aligned} \tag{10}$$

In the non-absorbing region, $H_k = 0$, so

$$\ln\ I_t^{\text{NA}} = \ln\ \bar{I}_0 + \sum_{n=0}^{\infty} p_n\ \cos[n(\omega t + \psi)]. \tag{11}$$

We first demodulate $\ln\ I_t^{\text{NA}}$ with reference signal $\cos(\omega t + \eta)$,

$$R_{1f}^{\text{NA}} = [\ln\ I_t^{\text{NA}} \times \cos(\omega t + \eta)] \otimes \text{lowpass} = \frac{1}{2} p_1\ \cos(\psi - \eta), \tag{12}$$

and try to seek the value of η so that $R_{1f}^{\text{NA}} = 0$. Assuming we have found such an η, at this time,

$$\psi - \eta = \frac{\pi}{2} + j\pi, \qquad j = 0, \pm 1, \pm 2, \cdots. \tag{13}$$

Secondly, we demodulate $\ln\ I_t$ with reference signal $\cos(2\omega t + 2\eta)$,

$$\begin{aligned}R_{2f} &= [\ln\ I_t \times \cos(2\omega t + 2\eta)] \otimes \text{lowpass} \\ &= \frac{1}{2} p_2\ \cos(2\psi - 2\eta) - \frac{1}{2} H_2\ \cos(2\psi + 2\phi - 2\eta).\end{aligned} \tag{14}$$

According to Eq. (13), $2\phi - 2\eta = (2j + 1)\pi$, thus

$$R_{2f} = -\frac{1}{2} p_2 + \frac{1}{2} H_2\ \cos(2\phi). \tag{15}$$

We can learn from Eq. (15) that the second harmonic in ln-WMS is naturally free of laser intensity $\bar{I}_0$, so it can be potentially used for remote sensing without cooperative reflectors. p_2 and ϕ

Table 1. Pseudocode of η-Seeking Algorithm.

1. **Initialize** $\eta = 0$, stride $s = \pi/4$, threshold $\varepsilon = 10^{-3}$, residuals $r = 1$.
2. while $r > \varepsilon$, repeat :
3. $R_{1f}^{\mathrm{NA}} = (\ln I_t^{\mathrm{NA}} \times \cos(\omega t + \eta)) \otimes$ lowpass
4. $R_{1f}^{\mathrm{NA}}[F] = (\ln I_t^{\mathrm{NA}} \times \cos(\omega t + \eta + s)) \otimes$ lowpass
5. $R_{1f}^{\mathrm{NA}}[B] = (\ln I_t^{\mathrm{NA}} \times \cos(\omega t + \eta - s)) \otimes$ lowpass
6. **if** $|R_{1f}^{\mathrm{NA}}| < |R_{1f}^{\mathrm{NA}}[F]|$ **and** $|R_{1f}^{\mathrm{NA}}| < |R_{1f}^{\mathrm{NA}}[B]|$:
7. $r \leftarrow$ mean of $|R_{1f}^{\mathrm{NA}}|$
8. **else** :
9. **if** $|R_{1f}^{\mathrm{NA}}[F]| < |R_{1f}^{\mathrm{NA}}|$ **and** $|R_{1f}^{\mathrm{NA}}[F]| < |R_{1f}^{\mathrm{NA}}[B]|$:
10. $r \leftarrow$ mean of $|R_{1f}^{\mathrm{NA}}[F]|$
11. $\eta \leftarrow \eta + s$
12. **else** :
13. $r \leftarrow$ mean of $|R_{1f}^{\mathrm{NA}}[B]|$
14. $\eta \leftarrow \eta - s$
15. $s \leftarrow s/2$

are related to inherent properties for a certain laser, so they are constant values at a constant modulation mode, and, when combined with Eq. (9), it is clear that R_{2f} is linear to CL with no limitation on absorbance.

Now we will discuss the η-seeking algorithm. According to Eq. (12), the problem is equivalent to looking for η so that $|p_1 \cos(\eta - \psi)/2| = 0$. Noticing that it is a periodic function and its period is π, we only have to seek the solution within the range of $\eta \in [-\pi/2, \pi/2)$. Within one period, $|p_1 \cos(\eta - \psi)/2|$ has only one maximum value and one minimum value, which are $|p_1/2|$ and zero, respectively, so we do not have to worry about falling into local minima. What we should do in the algorithm is to minimize $|R_{1f}^{\mathrm{NA}}|$ by varying η through iterations. More specifically, in each iteration, we should seek forward and backward starting from the initial value of η with shrinking strides until $|R_{1f}^{\mathrm{NA}}|$ is smaller than the preset threshold. The pseudocode is listed in Table 1.

3. Experiments and Results

To confirm the availability of ln-WMS, we applied it to measuring water vapor. The principle of choosing the probe absorption line is that there have to be non-absorbing spectral regions nearby, so that I_t^{NA} can be obtained and η can be retrieved. We chose the transition around 1392.2 nm as the probe. Figure 1 illustrates the absorption coefficient of water vapor around 1392.2 nm, from which we can see that there exists a

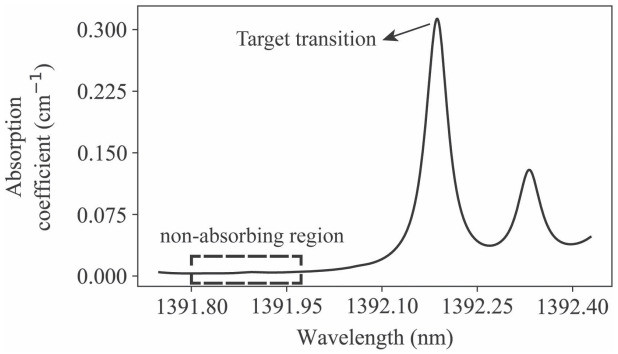

Fig. 1. Absorption coefficient of water vapor around 1392 nm (P = 1 atm, T = 296 K) based on HITRAN[19]. The non-absorbing region is indicated by the dotted rectangle.

spectral region where the absorption coefficient is approximately zero. It could be also known from Fig. 1 that there is slight spectral overlapping between the target transition and its adjacent absorption line, the main influence of which is to cause distortion to the side band of R_{2f}, as is illustrated in Fig. 2. The side band on the right of R_{2f} (sample points: 2000–3000) is not

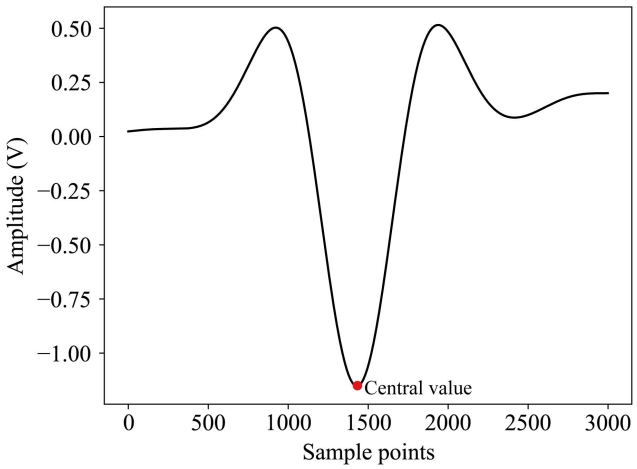

Fig. 2. Second harmonic R_{2f} demodulated from the absorption signal.

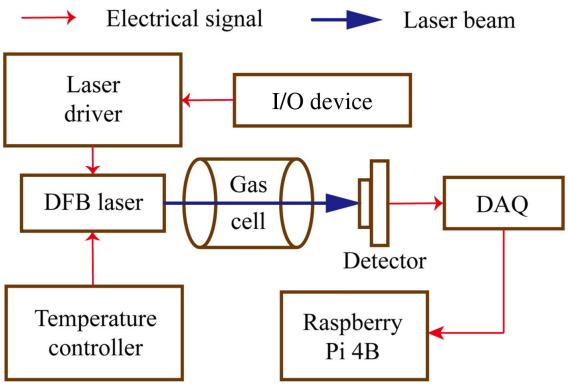

Fig. 3. Schematic of the experiment setup.

completely symmetrical with that on the left (sample points: 0–1000), where the former is distorted by the adjacent absorption line. The schematic of the experimental setup is illustrated in Fig. 3. In the experiment, a distributed feedback (DFB) diode laser (PL-DFB-1392-A-1-SA-14BF, LD-PD) emitting around 1392 nm was employed as the laser source. The laser beam was coupled into a multi-pass gas cell with an optical length of 8 m. The DFB laser was controlled by an integrated laser driver and temperature controller (LDTC 1020, Wavelength Electronics). The modulating signal composed of a 10 Hz saw tooth wave and a 5 kHz sine wave was generated by an NI-USB-6341 I/O device. The transmitted intensity was received by a photodiode detector (PDA20CS2, Thorlabs), whose output voltage was recorded by a data acquisition device (DAQ HATS 118, MCC) mounted on a Raspberry Pi 4B (CPU: Broadcom BCM2711B0 1.5 GHz, RAM: 4G). All of the computations including the demodulation processes and the η-seeking algorithm are executed on Raspberry Pi, and the programming language we used was Python 3.7.

A saturated steam at 0°C, 7°C, 14°C, 19°C, and 23°C was generated by a portable dew point generator (LI-610, LI-COR) and filled into the gas cell. According to Goff–Gratch equation, the volume fractions of water vapor at these temperatures are 0.6025%, 0.9878%, 1.5761%, 2.1668%, and 2.7709%, and the corresponding absorbance at the central frequency [i.e., $\alpha(\nu_0)CL$, where ν_0 is the central frequency of the absorption line] is 1.60, 2.23, 3.56, 4.90, and 6.26, respectively, calculated based on Fig. 1. For each measurement, we first tried to retrieve η with the η-seeking algorithm based on the non-absorbing region of the detected signal, as is illustrated in Fig. 4.

After that, the second harmonic R_{2f} was demodulated at phase 2η from the absorption signal, and the central values of R_{2f} were recorded. An illustration of the demodulated second harmonic is shown in Fig. 2. The measured central values of R_{2f} (ln-WMS-2f) at different volume fractions are plotted in Fig. 5, where the expression of the fitted line is $y = -75.872x - 0.2792$, and the goodness of fit is $R^2 = 0.9973$. For comparison, the responses of WMS-2f are plotted in the same figure. It is absolutely clear that under such large absorbance ln-WMS-2f is still linear to CL, however, this is not applicable to WMS-2f. As the volume fraction increases, WMS-2f rises with a shrinking slope in the beginning and then converts into descending. There have

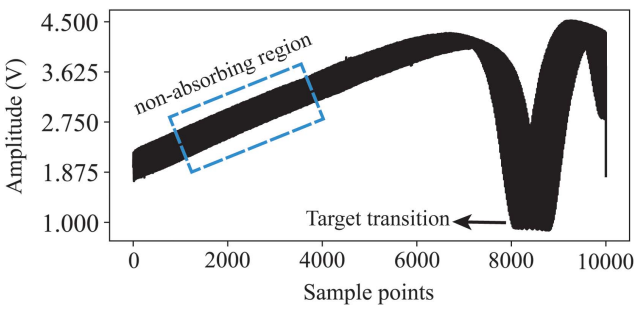

Fig. 4. Detected signal from the photodetector. The non-absorbing region is indicated by the dotted rectangle.

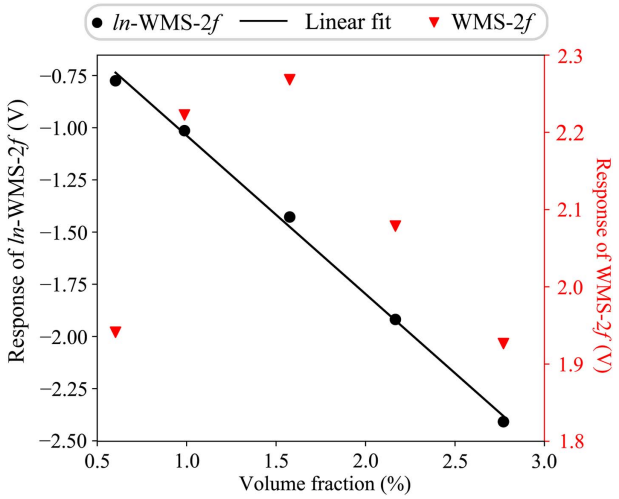

Fig. 5. Response of ln-WMS-2f (black dots) and WMS-2f (red inverted triangles). The black line represents the linear fit of ln-WMS-2f versus volume fraction.

not been studies on this kind of relationship as far as we know, maybe because such a non-monotonic response makes it pretty difficult to find a universal fitting function. It is a theoretical limitation for conventional WMS-2f to exhibit nonlinearity at large absorbance, which is because in the WMS-2f theory the linearity relies on the linear approximation of the Beer–Lambert Law [Eq. (3)], $I_t(t) = I_0(t)[1 - \alpha(\nu)CL]$, which is not valid for large absorbance.

4. Discussions

One of the keys to the implementation of ln-WMS is to determine the value of η. The values of η retrieved with the η-seeking algorithm during 90 s of continuous measurement are plotted in Fig. 6(a), from which it can be learned that for each measurement the retrieved η would be very different. From Fig. 6(b), we can learn that η mostly distributes near -0.3 rad and -0.15 rad, roughly $-\pi/10$ and $-\pi/20$. According to Eq. (13), there is a direct correlation between η and the phase of AM ψ. Unstable circuit response of the signal generator (NI-USB-6341) and the laser driver would lead to the instability of the modulation phase applied to the laser diode and then cause the fluctuation of ψ. Similarly, the inherent oscillation characteristics of the circuits would result into some certain distribution of ψ. Anyway, it is impossible to determine an accurate η in advance at all; thereby, it is necessary to retrieve η in real time during the measurements. In other words, the function of the η-seeking algorithm is to account for the instability of ψ, so that the second harmonic would be properly retrieved and could be expressed as Eq. (15) whatever ψ is. Figure 6(c) shows the mean of R_{1f}^{NA} for each measurement, namely, the residuals of the η-seeking algorithm, with which the validity of the algorithm is well illustrated. It took approximately 0.28 s (920 iterations roughly) for the algorithm to find η in each measurement.

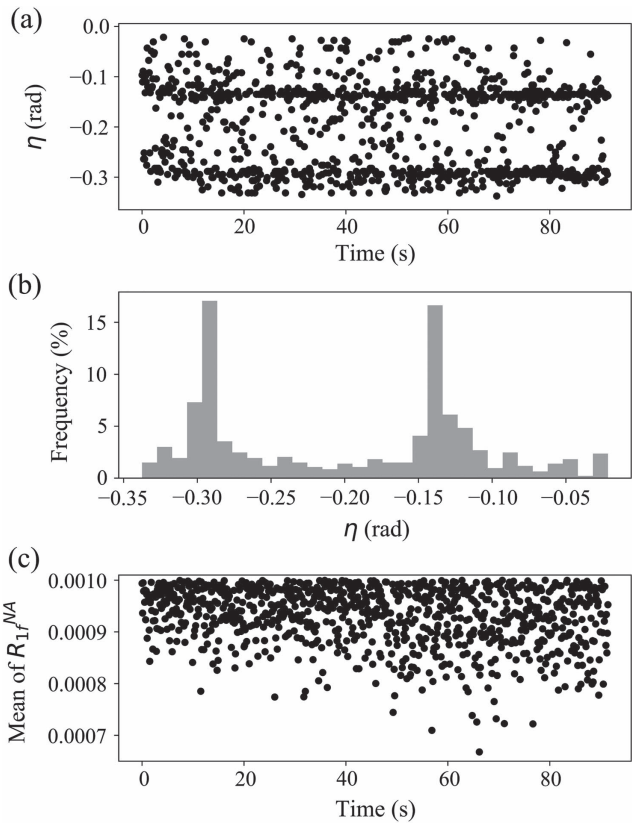

Fig. 6. (a) η retrieved with the η-seeking algorithm during 90 s of continuous measurement (0.1 s per measurement); (b) frequency distribution histogram of η; (c) mean of R_{1f}^{NA} for each measurement. The integral time of each point is 0.1 s.

The last thing worth mentioning is that, in applications where there is serious spectral congestion and non-absorbing regions like what Fig. 1 plots cannot be found, the non-absorbing intensity $\ln I_t^{\mathrm{NA}}$ can be obtained by splitting the laser into two beams and directly irradiating one of them onto the detector without passing through absorbers, at the cost of complicating the implementation of ln-WMS. Another potential solution to spectral overlapping is to operate at a reduced pressure, which will lead to a diminished width of the absorption spectrum.

5. Conclusion

In conclusion, this Letter demonstrates the novel ln-WMS technique, which can be regarded as an improvement of WMS-2*f*. It also needs linear calibration beforehand, but unlike the conventional WMS-2*f* method, it does not have the theoretical limitation of low absorbance. From the theory of ln-WMS, it can be confirmed that the linearity between ln-WMS-2*f* and the path-integrated concentration *CL* is established regardless of absorbance. To get the correct demodulating phase for the second harmonic, the η-seeking algorithm is proposed, working on minimizing the absolute value of the first harmonic within the non-absorbing spectral region. Experiments on water vapor offered convincing evidence that ln-WMS is valid even at large absorbance. This technique itself does not place theoretical limits, and it is especially applicable to large absorbance, such as measuring water vapor in ambient air.

Acknowledgement

This work was supported by the National Key Research and Development Program of China (No. 2018YFF0109600).

References

1. C. Ruan, D. Kong, J. Dai, K. Chen, S. Guo, and X. Wu, "High-resolution frequency-domain spectroscopy for water vapor with coherent and continuous terahertz wave," Chin. Opt. Lett. **17**, 073001 (2019).
2. J. Zou and F. Wang, "Simultaneous measurement of SO_2 and NO_2 concentration using an optical fiber-based LP-DOAS system," Chin. Opt. Lett. **18**, 021201 (2020).
3. J. Hodgkinson and R. P. Tatam, "Optical gas sensing: a review," Meas. Sci. Technol. **24**, 012004 (2013).
4. J. Li, B. Yu, W. Zhao, and W. Chen, "A review of signal enhancement and noise reduction techniques for tunable diode laser absorption spectroscopy," Appl. Spectrosc. Rev. **49**, 666 (2014).
5. K. K. Schwarm, C. L. Strand, V. A. Miller, and R. M. Spearrin, "Calibration-free breath acetone sensor with interference correction based on wavelength modulation spectroscopy near 8.2 μm," Appl. Phys. B **126**, 9 (2020).
6. J. Xia, F. Zhu, A. A. Kolomenskii, J. Bounds, S. Zhang, M. Amani, L. J. Fernyhough, and H. A. Schuessler, "Sensitive acetone detection with a mid-IR interband cascade laser and wavelength modulation spectroscopy," OSA Continuum **2**, 640 (2019).
7. G. B. Rieker, J. B. Jeffries, R. K. Hanson, T. Mathur, M. R. Gruber, and C. D. Carter, "Diode laser-based detection of combustor instabilities with application to a scramjet engine," Proc. Combustion Institute **32**, 831 (2009).
8. R. K. Hanson, P. A. Kuntz, and C. H. Kruger, "High-resolution spectroscopy of combustion gases using a tunable ir diode laser," Appl. Opt. **16**, 2045 (1977).
9. X. Chao, J. B. Jeffries, and R. K. Hanson, "Real-time, *in situ*, continuous monitoring of CO in a pulverized-coal-fired power plant with a 2.3 μm laser absorption sensor," Appl. Phys. B **110**, 359 (2013).
10. H. Li, A. Farooq, J. B. Jeffries, and R. K. Hanson, "Near-infrared diode laser absorption sensor for rapid measurements of temperature and water vapor in a shock tube," Appl. Phys. B **89**, 407 (2007).
11. C. Li, Y. Wu, X. Qiu, J. Wei, and L. Deng, "Pressure-dependent detection of carbon monoxide employing wavelength modulation spectroscopy using a Herriott-type cell," Appl. Spectrosc. **71**, 809 (2017).
12. C. Li, L. Shao, L. Jiang, X. Qiu, J. Wei, and W. Ma, "Simultaneous measurements of CO and CO_2 employing wavelength modulation spectroscopy using a signal averaging technique at 1.578 μm," Appl. Spectrosc. **72**, 1380 (2018).
13. J. Mikołajczyk, J. Wojtas, Z. Bielecki, T. Stacewicz, D. Szabra, P. Magryta, A. Prokopiuk, A. Tkacz, and M. Panek, "System of optoelectronic sensors for breath analysis," Metrol. Meas. Syst. **23**, 481 (2016).
14. G. B. Rieker, J. B. Jeffries, and R. K. Hanson, "Calibration-free wavelength-modulation spectroscopy for measurements of gas temperature and concentration in harsh environments," Appl. Opt. **48**, 5546 (2009).
15. A. J. McGettrick, K. Duffin, W. Johnstone, G. Stewart, and D. G. Moodie, "Tunable diode laser spectroscopy with wavelength modulation: a phasor decomposition method for calibration-free measurements of gas concentration and pressure," J. Lightwave Technol. **26**, 432 (2008).
16. W. Ding, L. Sun, L. Yi, and E. Zhang, "'Baseline-offset' scheme for a methane remote sensor based on wavelength modulation spectroscopy," Meas. Sci. Technol. **27**, 085202 (2016).
17. G. B. Rieker, H. Li, X. Liu, J. B. Jeffries, R. K. Hanson, M. G. Allen, S. D. Wehe, P. A. Mulhall, and H. S. Kindle, "A diode laser sensor for rapid, sensitive measurements of gas temperature and water vapour concentration at high temperatures and pressures," Meas. Sci. Technol. **18**, 1195 (2007).

18. G. Zhao, W. Tan, J. Hou, X. Qiu, W. Ma, Z. Li, L. Dong, L. Zhang, W. Yin, L. Xiao, O. Axner, and S. Jia, "Calibration-free wavelength-modulation spectroscopy based on a swiftly determined wavelength-modulation frequency response function of a DFB laser," Opt. Express **24**, 1723 (2016).
19. I. E. Gordon, L. S. Rothman, C. Hill, R. V. Kochanov, Y. Tan, P. F. Bernath, M. Birk, V. Boudon, A. Campargue, K. V. Chance, B. J. Drouin, J.-M. Flaud, R. R. Gamache, J. T. Hodges, D. Jacquemart, V. I. Perevalov, A. Perrin, K. P. Shine, M.-A. H. Smith, J. Tennyson, G. C. Toon, H. Tran, V. G. Tyuterev, A. Barbe, A. G. Császár, V. M. Devi, T. Furtenbacher, J. J. Harrison, J.-M. Hartmann, A. Jolly, T. J. Johnson, T. Karman, I. Kleiner, A. A. Kyuberis, J. Loos, O. M. Lyulin, S. T. Massie, S. N. Mikhailenko, N. Moazzen-Ahmadi, H. S. P. Müller, O. V. Naumenko, A. V. Nikitin, O. L. Polyansky, M. Rey, M. Rotger, S. W. Sharpe, K. Sung, E. Starikova, S. A. Tashkun, J. V. Auwera, G. Wagner, J. Wilzewski, P. Wcisło, S. Yu, and E. J. Zak, "The HITRAN2016 molecular spectroscopic database," J. Quantum Spectrosc. Radiat. Transfer **203**, 3 (2017).